**International Journal of Hydrological and Environmental for Sustainability**
**Volume 5, Issue 3, 247-262.**
e_ISSN: 2828-5050
https://www.journal.foundae.com/index.php/ijhes

# Machine-Learning-Based Vibration Classification of Inter-Module Connector Stiffness Loss in Modular Flood-Response Structures: A Simulation-Based Proof of Concept

**Sely Novita Sari***
Faculty of Engineering and Planning,
National Institute of Technology Yogyakarta,
INDONESIA

**Fitri Nugraheni**
Faculty of Engineering and Planning,
Islamic University of Indonesia,
INDONESIA

**Bagus Gilang Pratama**
Faculty of Engineering and Planning,
National Institute of Technology Yogyakarta,
INDONESIA

**Ignatius Adi Prabowo**
Built Environment and Surveying,
Universiti Teknologi Malaysia,
MALAYSIA

***Correspondence: E-mail:** sely.novita@itny.ac.id

**Article Info**

***Article history:***

Received: March 10, 2026
Revised: June 26, 2026
Accepted: August 17, 2026



**Abstract**

Ensuring the safety of modular facilities used for flood response and post-disaster sheltering requires reliable assessment of inter-module connections that may deteriorate under hydrodynamic loading, debris impact, repeated wetting, and corrosion. This study presents a simulation-based proof of concept for classifying connector residual stiffness from vibration response using machine learning. Flood-load analysis quantified hydrostatic, hydrodynamic, and debris-impact forces under five severity scenarios, which were hypothetically associated with seven prescribed connector-stiffness levels ranging from 100% to 5%. Only the stiffness-to-vibration relationship was physically simulated; the flood-exposure-to-stiffness relationship was assumed rather than experimentally validated. Finite element modal analysis in OpenSeesPy provided the first four natural frequencies and mode shapes, from which sixteen diagnostic features were derived. Gaussian perturbations generated 350 synthetic realizations from the seven deterministic stiffness states. To minimize data leakage, classifiers were evaluated using block-grouped cross-validation and compared with majority-class and second-mode-frequency baselines. Random Forest achieved the best multiclass performance, with a macro-F1 of 0.62 and balanced accuracy of 0.63, although early-stage deterioration classes remained difficult to distinguish. When reformulated as a binary severe/non-severe screening task, the model achieved 0.94 balanced accuracy with a 0.10 false-safe rate. These results demonstrate within-configuration separability under synthetic noise rather than field generalization. The proposed framework may support rapid condition screening of modular connections, but experimental validation of the degradation mapping, structural model, and sensing strategy is required before field implementation.

**Keywords:** machine learning, connector stiffness, vibration-based damage detection, finite element modelling, flood-response infrastructure

**To cite this article:** Sari, S, N., Nugraheni, F., Pratama, B, G. and Prabowo, I, A. (2026). Machine-Learning-Based Vibration Classification of Inter-Module Connector Stiffness Loss in Modular Flood-Response Structures: A Simulation-Based Proof of Concept. *International Journal of Hydrological and Environmental for Sustainability, 5*(3), 247-262. https://doi.org/10.58524/ijhes.v5i3.1456

## INTRODUCTION

Hydrometeorological hazards, and floods in particular, are among the most frequent and damaging natural disasters worldwide, and both their frequency and severity are projected to intensify under a changing climate (Mishra & Sadhu, 2023; Rözer et al., 2022). Floods repeatedly damage infrastructure, disrupt essential services, and threaten the safety of affected communities. Effective disaster response therefore depends on facilities that can be deployed rapidly in flood-affected areas and remain safe to occupy throughout the emergency. Modular structures prefabricated units assembled on site have become a widely used solution for flood-response shelters and emergency facilities because they can be erected quickly, reconfigured to local conditions, and later dismantled, relocated, and reused (Di Sarno & Forgione, 2024).

A defining feature of flood-response modular facilities is that they are deployed precisely in flood-prone zones and are frequently reused across multiple flood seasons. As a result, their connections accumulate damage over repeated exposure rather than from a single event. Each flood subjects the structure to hydrostatic pressure, hydrodynamic drag proportional to the square of the flow velocity, impulsive debris impact, and, at high water levels, buoyant uplift; between events, residual moisture and water-borne contaminants accelerate corrosion at the connectors. Because a modular assembly behaves as a single structural system only through its inter-module connections, the cumulative degradation of these connections unlike damage to a monolithic structure directly governs whether the facility remains safe. This recurring, cumulative nature of flood exposure is precisely what makes continuous condition assessment important for temporary and reusable emergency facilities, and it distinguishes the present problem from one-off structural assessment.

The condition of inter-module connections is difficult to monitor in practice. Visual inspection is subjective, requires trained personnel, and often cannot detect bolt loosening or connector stiffness loss before it becomes visible a limitation that is acute during and immediately after flood events, when access is constrained and rapid occupancy decisions are needed. Vibration-based structural health monitoring (SHM) offers an objective alternative, based on the principle that damage reduces stiffness and thereby alters dynamic parameters such as natural frequencies and mode shapes (Farrar et al., 2025; Sun et al., 2023). The specific link between connection loosening and a measurable drop in natural frequency has been demonstrated experimentally for bolted assemblies (He & Zhu, 2014), and machine learning has been applied successfully to vibration data for detecting and quantifying bolt loosening in steel-frame and multi-bolt structures (Chelimilla et al., 2023; Eraliev et al., 2022; Pal et al., 2022). In the flood domain specifically, vibration-based SHM is well established for detecting foundation scour and assessing bridge stability under hydrodynamic forces, increasingly combined with the Internet of Things and artificial intelligence for early warning during floods (Fitzgerald et al., 2019; Lin et al., 2021; Zarafshan et al., 2012). However, these strands of work have not been brought together for the specific problem of inter-module joint integrity in modular flood-response facilities, which remains largely unexamined.

Beyond safety, condition monitoring of modular facilities has a clear environmental-sustainability dimension that motivates this work. The principal sustainability advantage of modular construction that units can be reused across multiple deployments can only be realized safely if the structural integrity of the connections is known. A reliable monitoring framework would allow facility managers to make evidence-based reuse decisions, extend the service life of units that remain sound, avoid the premature scrapping and replacement of units whose condition is merely uncertain, and prioritize maintenance where it is genuinely needed. Each of these outcomes reduces material consumption and construction waste and supports the circular use of modular components, aligning the proposed framework with sustainable flood-disaster management.

**Table 1** positions the present study against representative prior work along five dimensions that are central to the problem addressed here: vibration-based modal analysis, machine-learning classification, application to modular construction, explicit treatment of the inter-module connector as the damage variable, and a flood or hydrological operating context. Vibration-based damage detection and machine-learning SHM are both mature, and bolted-connection diagnosis is well established for pipelines and steel frames; monitoring under flood loading has been addressed almost exclusively for bridge scour. Modular construction, however, appears in the multi-hazard design literature rather than in the monitoring literature, and no prior study combines all five dimensions.

**Table 1.** Positioning of the present study relative to representative prior work on vibration-based monitoring, bolted-connection diagnosis, and modular flood-response structures

| Representative prior work | Vibration / modal analysis | Machine learning | Modular structure | Inter-module connector | Flood / hydrological context |
|---|---|---|---|---|---|
| Sun et al. (2023) | ✓ | – | – | – | – |
| Farrar et al. (2025) | ✓ | ✓ | – | – | – |
| Malekloo et al. (2022) | ✓ | ✓ | – | – | – |
| He & Zhu (2014) | ✓ | – | – | ✓ | – |
| Eraliev et al. (2022); Pal et al. (2022) | ✓ | ✓ | – | ✓ | – |
| Chelimilla et al. (2023) | ✓ | ✓ | – | ✓ | – |
| Zarafshan et al. (2012); Fitzgerald et al. (2019) | ✓ | – | – | – | ✓ |
| Lin et al. (2021) | ✓ | ◐ | – | – | ✓ |
| Di Sarno & Forgione (2024) | – | – | ✓ | – | ✓ |
| **This study** | ✓ | ✓ | ✓ | ✓ | ✓ |

***Note:*** *✓= addressed; ◐ = partially addressed; – = not addressed. The flood/hydrological column refers to the operating context of the monitored structure, not to hydraulic modelling. Lin et al. (2021) are marked ◐ for machine learning because their system applies artificial-intelligence-of-things methods to real-time sensing and flood early warning rather than to classification of structural condition from modal features; Zarafshan et al. (2012) and Fitzgerald et al. (2019) diagnose scour from vibration response without a learning algorithm. In the present study the inter-module connector column denotes connector stiffness treated explicitly as the damage variable, and the flood context is an assumed exposure scenario rather than a physically coupled load path.*

The novelty of this study lies in positioning inter-module connection stiffness as the primary damage variable and classifying it directly from vibration response, while explicitly linking that variable to flood loading. To avoid overstating the contribution, the scope of each component is stated clearly. The flood load magnitudes and the finite element modal response are physically modeled. The mapping from cumulative flood exposure to connector stiffness is a hypothetical, engineering-judgment scenario adopted for demonstration, not a validated degradation law. No part of the framework has yet been validated against experimental or field data; the study is therefore a proof of concept. Within this scope, the objectives are (1) to quantify the flood-induced loads on a modular structure and define a transparent scenario mapping to connector degradation; (2) to develop and evaluate a machine-learning framework that classifies joint integrity from vibration features; and (3) to identify the modal features most sensitive to degradation, while assessing the limitations of the approach for early-stage damage. These objectives are pursued through four testable questions: (Q1) which modal features are most sensitive to prescribed connector-stiffness loss; (Q2) whether severe stiffness loss can be distinguished under realistic measurement noise; (Q3) whether a machine-learning classifier outperforms a simple threshold on the second-mode frequency; and (Q4) how strongly classification performance depends on the assumed noise level and on the validation strategy. Two distinct relationships are involved and are kept separate throughout: flood exposure causing connector deterioration, which is assumed here, and connector stiffness loss modifying modal properties, which is the only relationship physically simulated in the finite element model.

## METHOD

The methodology comprises three stages: (i) an analytical flood load analysis and its scenario mapping to connector degradation, (ii) finite element modeling with modal analysis, and (iii) machine-learning classification. **Figure 1** illustrates the physical configuration and the principal flood load mechanisms.

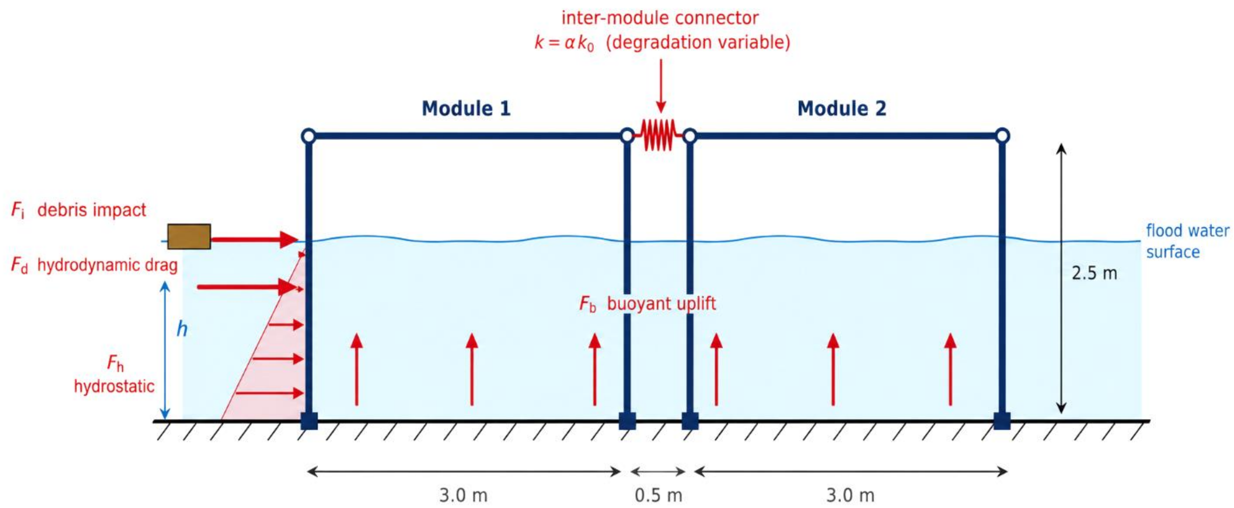


**Figure 1.** Physical configuration of the two-module assembly and the four principal flood load mechanisms acting on it: hydrostatic pressure ($F_h$), hydrodynamic drag ($F_d$), debris impact ($F_i$), and buoyant uplift ($F_b$). The inter-module connector, whose stiffness $k = \alpha k_0$ is the degradation variable, links the adjacent upper nodes

## Flood Loading Mechanisms and Scenario Definition

Four flood load types act on the structure (**Figure 1**): hydrostatic pressure ($F_h$), hydrodynamic drag ($F_d$), debris impact ($F_i$), and buoyant uplift ($F_b$). Hydrostatic and hydrodynamic forces were computed from standard hydraulic expressions, $F_h = ½\rho g h^2 b$ and $Fd = ½\rho CdAv^2$, where ρ is the water density, $g$ the gravitational acceleration (9.81 m/s$^2$), $h$ the inundation depth (m), $b$ the module width (3.0 m), $C_d$ the drag coefficient (1.2 for a rectangular body), $A$ the submerged frontal area, and $v$ the flow velocity (m/s). The submerged frontal area was taken as $A = b \times h$ in each scenario, assuming uniform flow over the wetted module face of height up to 2.5 m. A density of $\rho$ = 1,025 kg/m$^3$ was adopted to represent sediment-laden flood water; since the sediment concentration was not independently quantified, this value is only about 2.5% above the 1,000 kg/m$^3$ of clear water, so substituting clear-water density would change all computed forces by the same small factor and would not alter the relative severity ranking or any conclusion of this study. The computed forces are treated as simplified equivalent-static peak loads per event and are used as a relative severity index rather than as code-calibrated design loads.

The five severity scenarios (S1–S5 in **Table 2**) are design-scenario assumptions rather than site-specific measurements. The chosen depth–velocity combinations follow the widely used flood-hazard rating concept, in which hazard increases with the product of inundation depth and flow velocity: S1 ($h$ = 0.3 m, $v$ = 0.3 m/s) represents a shallow, low-velocity nuisance flood, while S5 ($h$ = 2.0 m, $v$ = 2.5 m/s) represents an extreme, high-velocity event with near-total submersion. The debris-impact force was estimated as $Fi = mdv/\Delta t$ and applied only when $v$ > 0.5 m/s, using a representative debris mass md = 450 kg (a medium floating object such as a small log or furniture item) and a contact duration $\Delta t = 0.1\ s$; these values are representative simplifications consistent with the order of magnitude of debris-impact provisions in flood load guidance (ASCE, 2022; FEMA, 2011) and are acknowledged as assumptions to be calibrated against site data in future work. Because the debris force is directly proportional to the debris mass and impact velocity and inversely proportional to the contact duration, it is highly sensitive to these assumptions: at the S5 velocity, varying the debris mass over 200–700 kg and the contact duration over 0.05–0.2 s changes the estimated impact force from about 2.5 kN to 35 kN. This range does not affect the condition-class ordering used here which follows the assumed stiffness mapping rather than the absolute force but it shows that the debris force cannot be treated as a precise design value, and a coefficient of restitution and variable impact location would widen the range further. Buoyant uplift acts vertically and was therefore excluded from the lateral-force totals; the load analysis and its conclusions are accordingly restricted to lateral-load effects. For completeness, the uplift was estimated as $Fb = \rho gVsub$, with $Vsub$ the submerged module volume (plan area ≈ b×3.0 m): it grows from about 27 kN at S1 to 181 kN at S5 and is reported as a separate column in **Table 2**. Under deep submersion (S4–S5) an uplift of this magnitude could reduce support reactions and influence sliding, overturning, connector force, and modal behaviour; a coupled treatment of buoyancy is therefore identified as important future work, and the present modal results should be read as conditional on the lateral-load, fixed-base idealization.

## Mapping of Flood Exposure to Connector Stiffness Degradation

Each severity scenario was associated with a residual connector stiffness factor $\alpha$ (the ratio of degraded to intact connector stiffness), ranging from $\alpha$ = 1.00 (intact) to $\alpha$ = 0.05 (near-total loss). It must be stated explicitly that this mapping is a hypothetical, engineering-judgment scenario adopted for a proof-of-concept demonstration; it is not derived from fatigue testing, a corrosion-kinetics model, or experimental stiffness measurements, and it should not be interpreted as a validated degradation law. The mapping rests on the qualitative and physically reasonable premise that the cumulative product of load magnitude and the number of flood cycles correlate with progressive fatigue- and corrosion-driven loss of connector stiffness: a single minor event causes negligible change ($\alpha \approx 1.00$), whereas many severe, fully submerged events drive the stiffness toward collapse ($\alpha \approx 0.05$). The role of the mapping in this study is solely to generate physically ordered condition states for the classification experiment; establishing a quantitatively validated load–degradation relationship through fatigue/corrosion modeling and testing is identified as essential future work in the Conclusion.

**Table 2.** Flood severity scenarios, computed lateral load components, and the hypothetical mapping to residual connector stiffness ($\alpha$) and operational condition class

| Scenario | $h$ (m) | $v$ (m/s) | $F_h$ (kN) | $F_d$ (kN) | $F_i$ (kN) | $F_{tot}$ (kN) | $F_b$ (kN) | Events | α | Condition class |
|---|---|---|---|---|---|---|---|---|---|---|
| S1 – Minor | 0.3 | 0.3 | 1.36 | 0.05 | 0.00 | 1.41 | 27.1 | 1 | 1.00 | Safe |
| S2 – Moderate | 0.6 | 0.8 | 5.43 | 0.71 | 3.60 | 9.74 | 54.3 | 3 | 0.80 | Monitoring required |
| S3 – Major | 1.0 | 1.2 | 15.08 | 2.66 | 5.40 | 23.14 | 90.5 | 5 | 0.60 | Repair required |
| S4 – Severe | 1.5 | 1.8 | 33.94 | 8.97 | 8.10 | 51.00 | 135.7 | 8 | 0.25 | Unfit for occupancy |
| S5 – Extreme | 2.0 | 2.5 | 60.33 | 23.06 | 11.25 | 94.64 | 181.0 | 12 | 0.05 | Relocation required |

***Note:*** *$F_h$ = hydrostatic, Fd = hydrodynamic drag, Fi = debris impact (applied when v > 0.5 m/s). The Events column gives the projected number of flood events assumed to accumulate in each scenario, which together with the load magnitude underlies the assumed α mapping. Fb is the buoyant uplift, reported separately because it acts vertically and is excluded from the lateral total Ftot. The load columns are computed quantities, whereas the Events, α, and Condition class columns are assumptions. Fb = buoyant uplift, computed as ρgVsub and reported separately because it acts vertically and is excluded from the lateral totals*

## Finite Element Modeling

The structure was modeled with the OpenSees finite-element framework via its Python interface, OpenSeesPy (Ozsarac et al., 2025) as two adjacent single-bay portal modules, each 3.0 m wide and 2.5 m tall, separated by a 0.5 m gap. The model comprises eight nodes (four fixed supports at the column bases and four upper nodes), six elastic beam-column elements (four columns and two roof beams), and one connector element linking the adjacent upper nodes of the two modules. All frame members were assigned a representative light square hollow section with structural-steel properties: modulus of elasticity $E$ = 200 GPa, density $\rho$ = 7,850 kg/m$^3$, cross-sectional area $A = 1.5 \times 10^{-3}$ m$^2$, and second moment of area $I = 5.0 \times 10^{-6}$ m$^4$. The section was specified directly in the model by its area and second moment of area rather than taken from a catalogue; these values correspond approximately to a 150 × 150 × 2.6 mm square hollow section ($A$ = 1,533 mm$^2$, $I = 5.55 \times 10^6$ mm$^4$), that is, a light, relatively slender member typical of prefabricated modular framing. The properties are representative rather than taken from a specific product, consistent with the proof-of-concept scope, and they are the values from which all modal results reported in **Table 2** were computed. Member self-mass was not activated in the element formulation: the entire inertia of the model is carried by the lumped nodal masses defined below, so the steel density does not enter the eigenvalue problem and is quoted only to identify the material. The resulting modal frequencies are therefore governed by the combination of these member properties and the lumped masses, which explains the relatively high second to fourth modal frequencies reported in **Table 2** for a structure of this size.

Lumped translational masses of 400 kg were assigned at each upper node to represent roof cladding and occupancy load, giving a total modelled mass of 1,600 kg for the two-module assembly. The column bases were fully fixed. The inter-module connection was modeled as a two-node elastic connector element joining the adjacent upper nodes (nodes 4 and 7) of the two modules, carrying axial and flexural stiffness in the plane of the frame so that it transmits the relative horizontal motion between the modules. The connector was assigned the same section properties as the frame members over the 0.5 m gap, so that its intact stiffness follows directly from the element formulation: the axial term is $k_0$,axial = EA/L = (200 GPa × 1.5 × $10^{-3}$ $m^2$)/0.5 m = 6.0 × $10^8$ N/m and the transverse (flexural) term is $k_0$,transverse = $12EI/L^3$ = (12 × 200 GPa × 5.0 × $10^{-6}$ $m^4$)/$(0.5\ m)^3$ = 9.6 × $10^7$ N/m, with a rotational stiffness EI/L = 2.0 × $10^6$ N·m/rad; degradation was simulated by scaling the connector's elastic modulus, $k = \alpha \cdot k_0$, with α taken from **Table 2**, so that α acts directly on the connector's axial and flexural stiffness while the frame members are unchanged.

The activated degrees of freedom are the two in-plane translations and the in-plane rotation of the connected nodes. The model is two-dimensional (ndm = 2, ndf = 3) with eight nodes and twelve free degrees of freedom after applying the twelve base restraints; frame members and the connector use the elasticBeamColumn element with a linear geometric transformation, and lumped translational masses are assigned at the four upper nodes. Eigenvalues were extracted with the fullGenLapack solver, and each mode shape was mass-orthogonal and was normalized to unit Euclidean norm over the eight translational sensor degrees of freedom before feature extraction. Because only eigenvalue (modal) analysis was performed, damping was not required and was not included, which is appropriate for undamped modal extraction. The analysis used OpenSeesPy 3.5 with all quantities in SI base units (N, m, kg); the simulation and machine-learning code is provided as supplementary material to support reproducibility. It should be noted that $k_0$ is a representative assumed value consistent with the proof-of-concept scope, and that a zero-length spring idealization would give a different frequency spectrum the connector-element model adopted here is the one that produced all results reported below.

## Degradation Scenarios and Class Mapping

Connector degradation was represented by seven stiffness factors (1.00, 0.80, 0.60, 0.40, 0.25, 0.10, 0.05) grouped into five operational condition classes (**Table 3**). The class labels are operational decision categories the action a facility manager would take rather than strict structural-code limit states. They were assigned by engineering judgment to reflect the decision relevant at each degradation level are Safe (no action), Monitoring required (heightened observation), Repair required (intervention before continued use), Unfit for occupancy (must not be occupied pending repair), and Relocation required (beyond economical repair). Two stiffness levels were grouped into a single class where both levels imply the same operational decision: $\alpha$ = 0.40 and 0.25 both render the unit unfit for occupancy, and $\alpha$ = 0.10 and 0.05 both warrant relocation. This grouping, while operationally meaningful, produces a deliberate class imbalance (100 samples each for the two severe classes versus 50 for the others) that is revisited when interpreting the classifier results and in the limitations discussed in the Conclusion.

**Table 3.** Mapping of connector stiffness factor to operational condition class

| Stiffness factor α | Stiffness loss (%) | Condition class | Samples |
|---|---|---|---|
| 1.00 | 0 | Safe | 50 |
| 0.80 | 20 | Monitoring required | 50 |
| 0.60 | 40 | Repair required | 50 |
| 0.40 | 60 | Unfit for occupancy | 50 |
| 0.25 | 75 | Unfit for occupancy | 50 |
| 0.10 | 90 | Relocation required | 50 |
| 0.05 | 95 | Relocation required | 50 |
| **Total** | | | **350** |

## Modal Analysis, Feature Extraction, and Classification

Modal analysis yielded the natural frequencies and mode shapes of the first four modes. For each mode, four features were computed relative to the intact state natural frequency, frequency ratio, frequency shift, and the Modal Assurance Criterion (MAC) (Le & Goo, 2020) giving sixteen features per sample. To emulate sensor and modal-identification uncertainty and to augment the dataset, Gaussian noise was added independently to the frequencies and mode shapes, with 50 realizations per scenario, producing 350 samples. The perturbation was multiplicative for the natural frequencies (each frequency scaled by $1 + \varepsilon$, $\varepsilon \sim N(0, 0.02^2)$) and additive and independent for each mode-shape coordinate ($\varepsilon \sim N(0, 0.03^2)$ applied to the unit-normalized amplitude), after which each perturbed mode shape was renormalized to unit Euclidean norm. The distributions were untruncated and no sensor-to-sensor correlation was imposed. Because the perturbations are applied coordinate-wise and the vectors are then renormalized, modal orthogonality is not enforced; the perturbed shapes are therefore best interpreted as noisy measurements of the underlying modes rather than as exact eigenvectors of a perturbed system. Since modes 3 and 4 are closely spaced and could in principle exchange order between degradation states, modes were paired across states by maximum MAC with respect to the intact state before any feature was computed, ensuring that the same physical mode is compared throughout. The MAC itself was evaluated between each perturbed mode shape and the intact-state shape of the same configuration; being normalized by the vector norms and squaring the inner product, it is insensitive to scaling and to sign ambiguity. The noise levels (standard deviation of 2% for frequencies and 3% for mode shapes) were selected to represent the order of magnitude of identification uncertainty reported for ambient-vibration and low-cost-sensor SHM, in which environmental and operational variability typically perturbs identified frequencies by a few percent (Farrar et al., 2025); they are nominal assumptions rather than values calibrated to a specific sensor.

Classification used Random Forest (Halabaku & Bytyçi, 2024), a Support Vector Machine with an RBF kernel (Cortes & Vapnik, 1995), and k-Nearest Neighbors (Hao & Ho, 2019), together with three deliberately simple reference methods logistic regression, a single decision tree, and a one-feature threshold on the second-mode frequency and a majority-class baseline, so that the added value of the machine-learning models could be judged. Because connector stiffness is continuous and the condition classes are ordered, the nominal multiclass framing is a simplification, and regression or ordinal modeling is noted as a more natural alternative for future work. Class weighting inversely proportional to class frequency was applied to counter the imbalance between the severe and early-stage classes, and all preprocessing was carried out inside a pipeline whose standardizer was fitted only on the training partition of each fold, preventing leakage through scaling. Hyperparameters were set to commonly used values (Random Forest: 300 trees; SVM: $C = 10$, RBF kernel; kNN: k = 5); an exhaustive search was not performed and is noted as a limitation, and a fixed random seed (42) was used throughout for reproducibility. Because the 350 samples are noisy realizations of only seven deterministic stiffness states, evaluation used leakage-free block-grouped five-fold cross-validation: within each state the 50 realizations were divided into blocks, and whole blocks were held out so that no realization of a held-out block appeared in training, while every class remained present in every training fold. Performance was reported with accuracy, balanced accuracy, macro-F1, per-class precision/recall/F1, the Matthews correlation coefficient, a safety-oriented false-safe rate, the row-normalized confusion matrix, and permutation feature importance.

This grouped design directly addresses the principal methodological risk of the study. Had a plain random split been used, near-duplicate noisy realizations of the same deterministic state would have appeared on both sides of the split and inflated the apparent performance. The block-grouped evaluation removes that replica leakage, and the comparison against the simple baselines and the majority-class reference makes the modest size of the machine-learning advantage explicit. The remaining, more fundamental limitation that all realizations still derive from a single structural configuration cannot be removed by resampling alone and would require multiple independently simulated or physically tested configurations; the reported values should therefore still be read as within-configuration separability under synthetic noise rather than as field generalization.

# RESULTS AND DISCUSSION

## Flood Load Analysis

The computed load components show that the total lateral force rises from 1.4 kN (S1) to 94.6 kN (S5), an increase of nearly two orders of magnitude. The breakdown clarifies the mechanism: hydrostatic pressure dominates at low velocities (e.g., 1.36 of 1.41 kN at S1), whereas hydrodynamic drag and debris impact grow rapidly with velocity and together exceed the hydrostatic component at S5 (23.06 and 11.25 kN versus 60.33 kN). Debris impact is zero at S1 because the flow velocity (0.3 m/s) is below the 0.5 m/s threshold adopted for debris mobilization. In the finite element idealization, these lateral forces are transferred through the roof beams of each module to the upper nodes, where the inter-module connector links the two units; because the connector is the most flexible load path between the modules, the relative displacement it must accommodate is expected to concentrate demand at the connection; this is stated as a conceptual assumption motivating the choice of connector stiffness as the governing degradation variable, since no static, stress, or force-transfer analysis was performed to demonstrate it quantitatively. A fully coupled fluid–structure transfer analysis was beyond the present scope and is identified as future work.

## Modal Response Across The First Four Modes

Examining all four extracted modes (**Table 4**) shows that the diagnostic information is concentrated in the second mode. The first mode (≈ 6 Hz) corresponds to a global lateral sway of the two-module assembly and is almost insensitive to connector degradation (6.06 → 5.75 Hz). The third and fourth modes (≈ 87 Hz) are local member modes and remain essentially constant. Only the second mode changes substantially, falling from 76.1 Hz at $\alpha$ = 1.00 to 40.7 Hz at $\alpha$ = 0.05 (a 46% reduction, **Figure 2**). Physically, the second mode is an anti-symmetric mode involving relative motion between the two modules across the connection; its deformation is therefore concentrated at the connector, making its frequency the most sensitive indicator of joint stiffness loss. This modal interpretation explains, and is consistent with, the feature-importance results reported below.

**Table 4.** Mean natural frequencies (Hz) of the first four modes at each connector stiffness factor

| Stiffness factor α | Mode 1 | Mode 2 | Mode 3 | Mode 4 |
|---|---|---|---|---|
| 1.00 | 6.06 | 76.08 | 86.90 | 87.68 |
| 0.80 | 6.03 | 75.37 | 87.65 | 87.22 |
| 0.60 | 6.04 | 74.30 | 86.78 | 87.18 |
| 0.40 | 6.01 | 71.34 | 87.35 | 87.52 |
| 0.25 | 5.95 | 66.61 | 87.09 | 86.92 |
| 0.10 | 5.83 | 52.80 | 87.33 | 87.04 |
| 0.05 | 5.75 | 40.65 | 87.19 | 87.14 |

***Note:*** *Values are means over the 50 noisy realizations per state; only the second mode varies appreciably with α*

**Figure 3** shows the second-mode shape at three representative states. The mode is anti-symmetric are the two modules move in opposition across the connection, so the modal deformation concentrates at the connector. As α decreases, the relative motion across the joint grows while the frequency falls, which explains why second-mode features dominate the classification.

The trend is markedly nonlinear are the second-mode frequency is relatively flat between α = 1.00 and 0.60 and drops steeply only below α = 0.40. This threshold behavior, which is also reported for scour-induced and bolt-loosening stiffness loss (Prendergast & Gavin, 2014; He & Zhu, 2014), is the underlying reason why early-stage degradation is difficult to distinguish using the present structural model, modal features, and assumed noise levels, as the classification results confirm. This threshold behavior may be specific to the symmetric two-module portal configuration and the prescribed stiffness range analysed here, and should not be generalized to modular structures as an intrinsic property. It should also be noted that only the fundamental mode (6.06 Hz in the intact state) lies in the range usually expected for a building-scale structure; modes 2 to 4 fall between about 76 and 88 Hz because they involve local, anti-symmetric deformation of comparatively stiff members carrying lumped masses at only four nodes. These higher frequencies are therefore a consequence of the idealization rather than a prediction of the response of a real modular facility, and experimental modal comparison is required before the absolute values are relied upon.

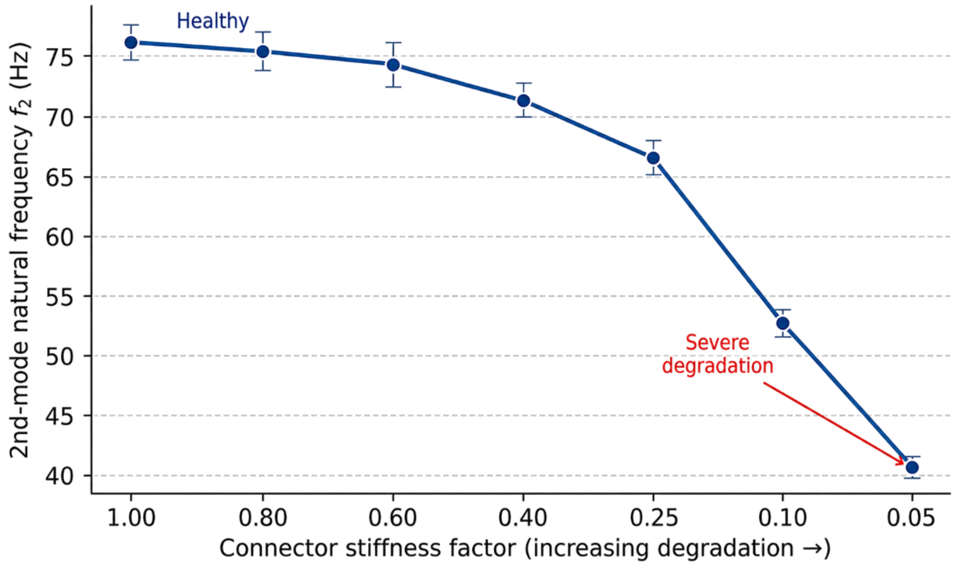


**Figure 2.** Shift in the second-mode natural frequency with decreasing connector stiffness factor

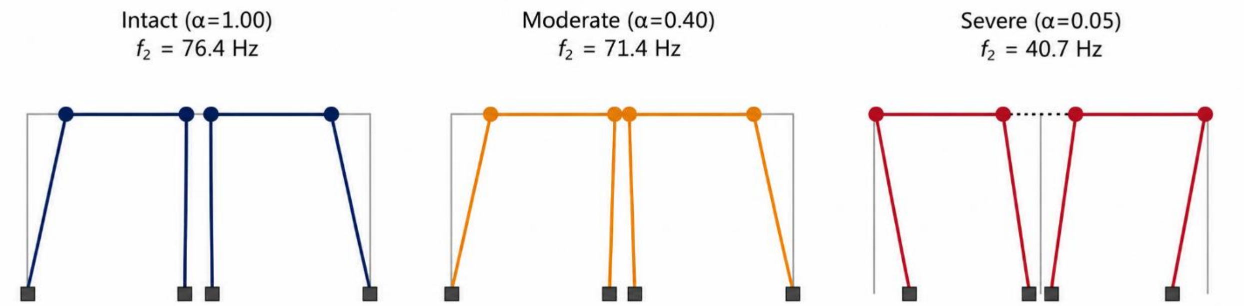


**Figure 3.** Second-mode shape at three degradation states (grey = undeformed, coloured = modal displacement, dotted line = inter-module connector). The mode is anti-symmetric across the connection at all states

## Classifier Performance

Because the 350 samples are noisy realizations of only seven deterministic stiffness states, a random train–test split would place near-duplicate realizations of the same state on both sides of the split and yield optimistic performance. All results reported here therefore use leakage-free, block-grouped five-fold cross-validation, in which the noisy realizations of each state are divided into blocks and whole blocks are held out, so that no realization of a held-out block appears in training; the standardizer is fitted within each training fold only, inside a pipeline. Under this evaluation (**Figure 4**, **Table 5**), Random Forest gave the best overall result with a mean accuracy of 0.73, but its balanced accuracy (0.63) and macro-F1 (0.62) show that the five classes are not discriminated uniformly. Crucially, Random Forest was only modestly better than the simpler reference methods: logistic regression reached macro-F1 0.60, a decision tree 0.58, and even a single-feature threshold on the second-mode frequency 0.61, whereas a majority-class baseline reached only 0.09. Machine learning thus provides a measurable but limited advantage over a simple frequency threshold on this dataset. All performance values should be read as upper-bound estimates of within-configuration separability under synthetic noise, not as estimates of field generalization.

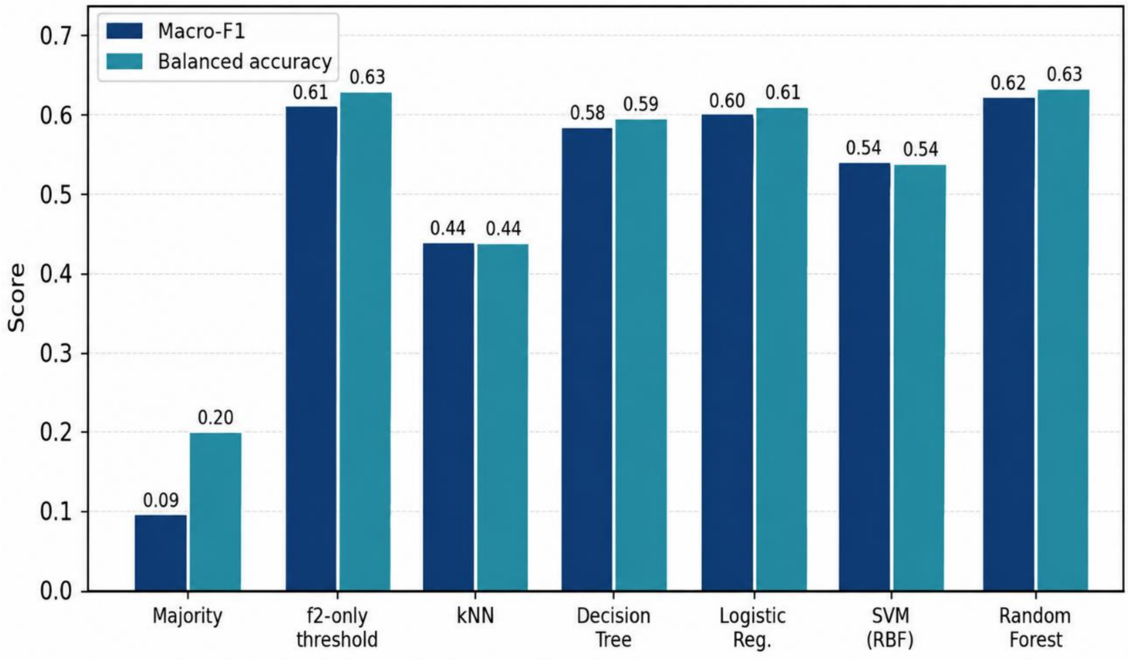


**Figure 4.** Leakage-free comparison of classifier performance (macro-F1 and balanced accuracy), including majority-class and single-feature-threshold baselines

**Table 5.** Overall classifier performance under leakage-free block-grouped five-fold cross-validation, including simpler reference baselines

| Model | Accuracy (5-fold) | Balanced accuracy | Macro-F1 |
|---|---|---|---|
| Random Forest | 0.726 ± 0.019 | 0.632 | 0.620 |
| Logistic regression | 0.700 ± 0.024 | 0.606 | 0.601 |
| Decision tree | 0.691 ± 0.043 | 0.592 | 0.584 |
| $f_2$-only threshold | 0.706 ± 0.065 | 0.630 | 0.613 |
| SVM (RBF) | 0.634 ± 0.041 | 0.536 | 0.539 |
| kNN (k = 5) | 0.537 ± 0.046 | 0.440 | 0.438 |
| Majority baseline | 0.286 ± 0.000 | 0.200 | 0.089 |

The per-class metrics from the leakage-free evaluation (**Table 6**) make the imbalance explicit. The two severe classes are recovered well within the synthetic test data (Relocation required: precision/recall/F1 = 1.00; Unfit for occupancy 0.88/0.92/0.90), whereas the early-stage classes are weak (Monitoring required: 0.37/0.36/0.36; Repair required: 0.42/0.34/0.38) and the Safe class is moderate (0.47/0.54/0.50). Quantifying the safety-critical errors directly, 10% of genuinely degraded samples were misclassified as Safe (false-safe rate), and only 4% of the two severe classes were missed as non-severe; the corresponding Matthews correlation coefficient is 0.65. In the context of structural-safety monitoring, these per-class results matter more than the aggregate accuracy: a false "Safe" prediction is far more consequential than a conservative over-warning. The framework should therefore be understood as a tool for screening severe, decision-critical degradation supporting evacuation, closure, or relocation decisions and rapid post-flood triage rather than as an early-warning system for incipient damage, for which its current sensitivity is insufficient.

**Table 6.** Per-class precision, recall, and F1-score for the Random Forest model, from leakage-free block-grouped cross-validation (out-of-fold predictions)

| Condition class | Precision | Recall | F1-score | Support |
|---|---|---|---|---|
| Safe | 0.47 | 0.54 | 0.50 | 50 |
| Monitoring required | 0.37 | 0.36 | 0.36 | 50 |
| Repair required | 0.42 | 0.34 | 0.38 | 50 |
| Unfit for occupancy | 0.88 | 0.92 | 0.90 | 100 |
| Relocation required | 1.00 | 1.00 | 1.00 | 100 |

## Confusion Matrix Analysis

The row-normalized confusion matrix (**Figure 5**) shows the severe classes recovered well within the synthetic test split while the early-stage classes are frequently interchanged. This pattern is physically explainable the small modal changes below 40% stiffness loss approach the noise level (see the modal response subsection above) but it nonetheless represents a genuine limitation of the present feature set and classifier in distinguishing early-stage degradation, and is described here as such rather than dismissed.

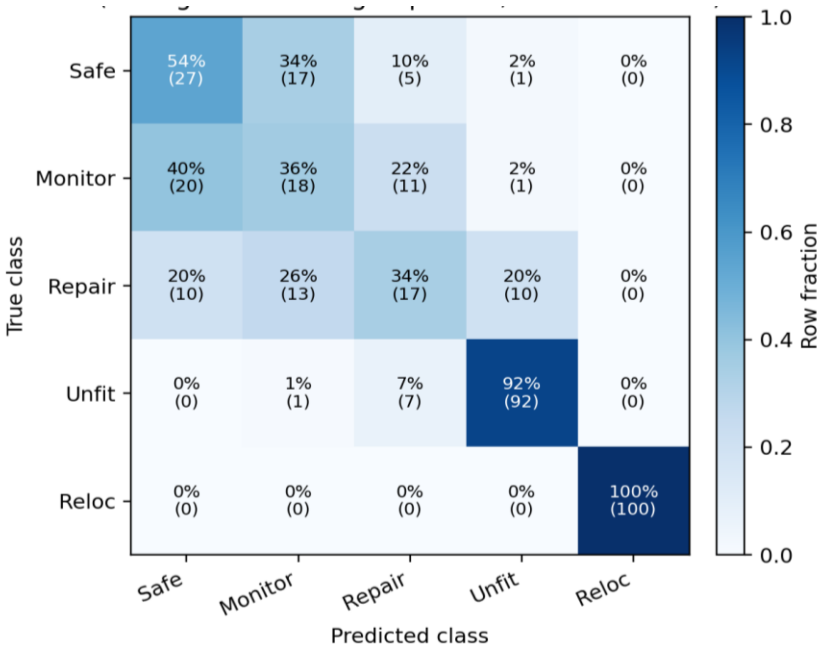


**Figure 5.** Random Forest confusion matrix from leakage-free block-grouped cross-validation, row-normalized (percentages) with sample counts in parentheses

The practical consequence of these confusions deserves emphasis. The most safety-critical error would be classifying a genuinely degraded unit (Repair required) as Safe or Monitoring required, which could lead to a hazardous unit remaining in service. Conversely, confusions among the lighter classes that err toward greater caution are operationally tolerable. For deployment, this asymmetry argues for a conservative decision rule for example, treating any ambiguous early-stage prediction as warranting physical inspection and for combining the classifier output with the flood-exposure context discussed below so that severe flood loading automatically raises the assessment threshold.

## Feature Importance

Because the frequency-derived features are strongly correlated (see below) and impurity-based importance can be biased for correlated predictors, feature importance was assessed with permutation importance computed on held-out configurations (**Figure 6**). It confirms the modal interpretation of the modal response subsection: the second-mode features (MAC2, $f_{shift2}$, and $f_{ratio2}$) carry essentially all of the usable discriminative information, while the first-, third-, and fourth-mode features contribute little or nothing. This consistency between the physics (mode 2 governs relative inter-module motion) and the data-driven importance lends credibility to the result and indicates that monitoring effort and sensor placement could be concentrated on capturing the second-mode response.

This finding should not be over-generalized, however. The dominance of the second mode is specific to the simplified, symmetric two-module portal configuration analyzed here. Different module layouts, boundary conditions, connection types, and mass distributions could shift the joint-sensitive mode elsewhere in the spectrum. The dominance of second-mode features should therefore be interpreted as configuration-specific and requires further validation for other modular layouts and connection systems. It should also be noted that the frequency, frequency-ratio, and frequency-shift features of a given mode are exact algebraic transforms of one another: for the second mode, the Pearson correlation between $f_{ratio2}$ and $f_{shift2}$ is −1.00 and that between $f_2$ and MAC2 is 0.91. These features are thus redundant; a reduced eight-feature set retaining only the natural frequency and MAC of each mode reproduced most of the severe-screening performance (balanced accuracy 0.92 versus 0.94), and the redundant frequency features are retained here only for continuity with the full feature set.

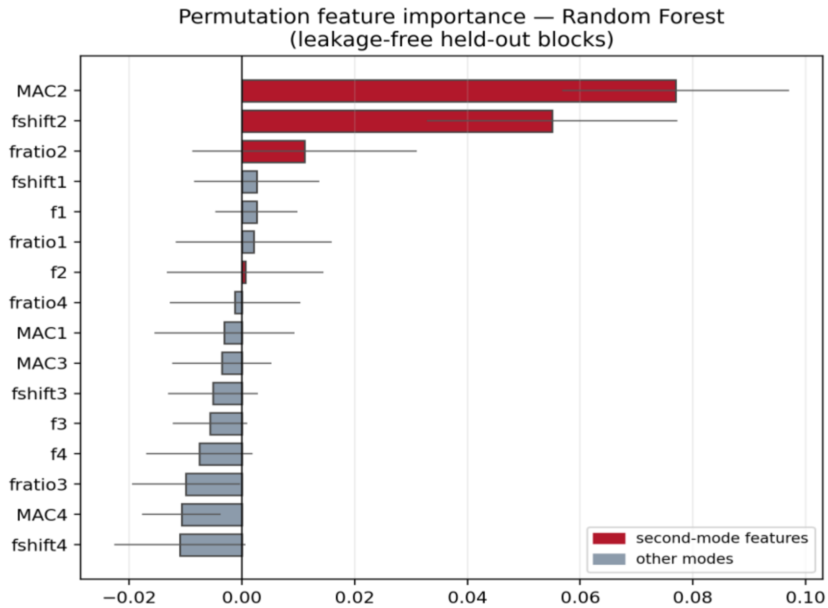


**Figure 6.** Permutation feature importance for the Random Forest model, computed on held-out configurations (mean decrease in macro-F1; error bars are standard deviations). Feature abbreviations: *f* = natural frequency, $f_{ratio}$ = frequency ratio, $f_{shift}$ = frequency shift, MAC = Modal Assurance Criterion; the trailing digit is the mode number.

### Sensitivity to The Assumed Noise Level

Because the 2% frequency and 3% mode-shape noise levels are assumptions rather than measured sensor characteristics, the entire leakage-free pipeline was repeated at four noise levels (**Figure 7**). Five-class macro-F1 falls steadily from 0.79 at 1% frequency noise to 0.50 at 5%, confirming that the multi-class result is strongly noise-dependent. The severe-versus-non-severe screening task is far more robust, remaining above 0.85 balanced accuracy across the whole range and approaching 1.00 at the lowest noise level. This contrast reinforces the main conclusion: the framework is defensible as a severe-damage screening tool rather than a five-class diagnostic, and the reported early-stage performance must be read as conditional on the assumed noise level.

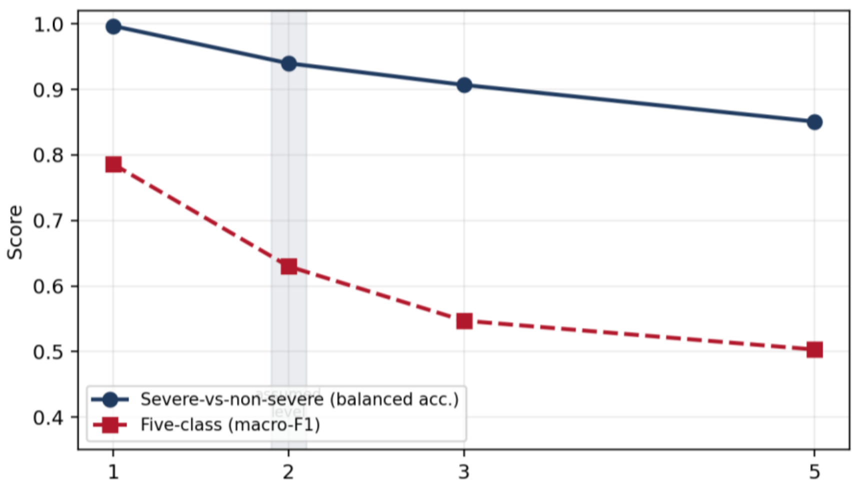


**Figure 7.** Sensitivity of leakage-free classification performance to the assumed synthetic sensor-noise level; the shaded band marks the level assumed in the main analysis.

**Implications for Integrated, Sustainable Flood-Response Monitoring**

The results support an integrated monitoring approach that combines vibration-based SHM with hydrological and environmental sensing, as advocated in recent literature. (Malekloo et al., 2022) describe how machine learning, the Internet of Things, and SHM can be fused into a single smart-infrastructure framework, and (Lin et al., 2021) demonstrated on scour-critical bridges that combining water-level and flow-velocity triggers with structural-vibration data reduces false alarms and improves the timeliness of flood early warnings. Translating this to modular flood-response facilities, the joint-integrity classifier would be embedded in an IoT platform alongside water-level and flow-velocity sensors: a detected severe flood (S4–S5) would automatically trigger a structural assessment and raise the conservatism of the decision rule, while minor events would invoke only low-frequency monitoring, conserving the energy and bandwidth that constrain battery-powered disaster deployments.

Crucially for the scope of this journal, such monitoring directly serves environmental sustainability. By providing objective evidence of structural condition, the framework enables: (i) safe, evidence-based reuse of modular units after flood exposure rather than precautionary disposal; (ii) extension of facility service life through condition-based rather than time-based replacement; (iii) maintenance prioritization that targets genuinely degraded connections; (iv) reduction of construction and demolition waste; and (v) support for the circular use of modular components across successive disasters. In this way, structural monitoring becomes an enabler of the resource efficiency that makes modular flood-response infrastructure sustainable in the first place.

Realizing these benefits in the field will require addressing several practical needs not covered by the present simulation: optimal accelerometer placement (informed here by the second-mode result), reliable data transmission and power supply in flood conditions, periodic sensor calibration, standardized inspection protocols to confirm classifier outputs, and the establishment of quantitative decision thresholds for the Safe, Repair, Unfit, and Relocation categories. These are prerequisites for translating the proof of concept into a deployable system.

## LIMITATIONS

Seven limitations bound the findings of this study and should be read together with the results. First, the flood-exposure-to-stiffness relationship is hypothetical: it rests on engineering judgement rather than fatigue testing, corrosion kinetics, or measured stiffness loss, and only the connector-stiffness-to-vibration relationship is physically simulated. Second, a single simplified structural configuration was analysed a two-dimensional, symmetric, fixed-base two-module portal with one connector, without cladding or diaphragm stiffness, bracing, or geometric nonlinearity so the results cannot be generalized to other layouts, connection types, damage locations, or three-dimensional behaviour. Third, the dataset consists of synthetic noisy replicas of only seven deterministic stiffness states rather than independent structures; block-grouped validation removes replica leakage but is no substitute for independently simulated or physically tested configurations. Fourth, the reported performance is therefore an upper-bound estimate of within-configuration separability under synthetic noise, and the advantage of machine learning over a simple second-mode threshold is modest. Fifth, no experimental or field validation was performed. Sixth, the operational class labels were assigned by judgement and are not derived from structural-code criteria, connection-capacity analysis, or reliability limit states, so they should be read as ordered condition levels rather than validated safety thresholds. Seventh, the sustainability benefits discussed above were not quantified: no life-cycle assessment, embodied-carbon comparison, or waste-reduction estimate was carried out.

## CONCLUSION

This study presented a simulation-based proof of concept that links flood loading, connector stiffness degradation, vibration response, and machine-learning classification into a single framework for assessing inter-module joint integrity in modular flood-response facilities. Within its simulated scope, and under leakage-free evaluation, the framework separated the two severe condition classes with high F1 scores within the present synthetic and potentially optimistic test data, and screened severe from non-severe states with about 0.94 balanced accuracy and a 0.10 false-safe rate. The second mode governing relative motion between the modules carried most of the diagnostic information, while the early-stage classes could not yet be reliably distinguished. The main contribution is therefore the identification of a connector-sensitive modal feature and a demonstration that it supports screening of severe stiffness loss, rather than a deployable multi-class classification system. The framework is therefore best positioned as a rapid screening and triage tool for severe post-flood conditions, not as an incipient-damage early-warning system, and it must be regarded as a proof of concept rather than a field-ready method. Its potential contribution to sustainable flood-disaster management is to enable evidence-based reuse and condition-based maintenance of modular units, thereby reducing premature replacement and construction waste. Realizing this potential requires, as essential prerequisites rather than optional extensions: (i) experimental validation on physical modular prototypes; (ii) calibration of the flood-exposure-to-stiffness mapping through fatigue and corrosion testing; (iii) integration of accelerometers with water-level and flow-velocity sensors in an IoT decision-support platform; (iv) testing across different connection types, damage locations, and module layouts; (v) development of quantitative decision thresholds for each condition class; (vi) sensitivity analysis with respect to the flood-load and connector-stiffness assumptions and a leakage-free, group-wise validation; and (vii) explicit evaluation of the sustainability benefits of reuse and service-life extension. Addressing these needs would move the framework from a demonstrated concept toward a deployable, sustainable monitoring system for resilient modular flood-response infrastructure.

## AUTHOR CONTRIBUTIONS

Conceptualization, SNS and FN; methodology, SNS and BGP; software, SNS; validation, SNS and IAP; formal analysis, SNS and FN; investigation, BGP; resources, SNS and FN; data curation, SNS; writing—original draft preparation, SNS; writing—review and editing, SNS and FN; visualization, SNS; supervision, SNS and IAP; project administration.

## ACKNOWLEDGMENT

The authors sincerely thank the reviewers for their valuable comments and constructive suggestions, which have significantly improved the quality and clarity of this manuscript.

## CONFLICTS OF INTEREST

The authors declare no conflict of interest concerning the publication of this article. The authors also confirm that the data and the article are free of plagiarism.

## REFERENCES

ASCE. (2022). Minimum Design Loads and Associated Criteria for Buildings and Other Structures (ASCE/SEI 7-22).

Chelimilla, N., Chinthapenta, V., Kali, N., & Korla, S. (2023). Review on recent advances in structural health monitoring paradigm for looseness detection in bolted assemblies. Structural Health Monitoring, 22(6), 4264–4304. https://doi.org/10.1177/14759217231158540

Cortes, C., & Vapnik, V. (1995). Support-vector networks. Machine Learning, 20(3), 273–297. https://doi.org/10.1007/BF00994018

Di Sarno, L., & Forgione, R. (2024). Innovative steel modular housing system for multiple natural hazard mitigation. International Journal of Disaster Risk Reduction, 111, 104734. https://doi.org/10.1016/j.ijdrr.2024.104734

Eraliev, O., Lee, K.-H., & Lee, C.-H. (2022). Vibration-Based Loosening Detection of a Multi-Bolt Structure Using Machine Learning Algorithms. Sensors, 22(3), 1210. https://doi.org/10.3390/s22031210

Farrar, C. R., Dervilis, N., & Worden, K. (2025). The Past, Present and Future of Structural Health Monitoring: An Overview of Three Ages. Strain, 61(1). https://doi.org/10.1111/str.12495

FEMA. (2011). Coastal Construction Manual (FEMA P-55, Vol. II).

Fitzgerald, P. C., Malekjafarian, A., Bhowmik, B., Prendergast, L. J., Cahill, P., Kim, C.-W., Hazra, B., Pakrashi, V., & O'Brien, E. J. (2019). Scour Damage Detection and Structural Health Monitoring of a Laboratory-Scaled Bridge Using a Vibration Energy Harvesting Device. Sensors, 19(11), 2572. https://doi.org/10.3390/s19112572

Halabaku, E., & Bytyçi, E. (2024). Overfitting in Machine Learning: A Comparative Analysis of Decision Trees and Random Forests. Intelligent Automation & Soft Computing, 39(6), 987–1006. https://doi.org/10.32604/iasc.2024.059429

Hao, J., & Ho, T. K. (2019). Machine Learning Made Easy: A Review of Scikit-learn Package in Python Programming Language. Journal of Educational and Behavioral Statistics, 44(3), 348–361. https://doi.org/10.3102/1076998619832248

He, K., & Zhu, W. D. (2014). Detecting Loosening of Bolted Connections in a Pipeline Using Changes in Natural Frequencies. Journal of Vibration and Acoustics, 136(3). https://doi.org/10.1115/1.4026973

Le, V. T., & Goo, N. S. (2020). Dynamic Characteristics and Damage Detection of a Metallic Thermal Protection System Panel Using a Three-Dimensional Point Tracking Method and a Modal Assurance Criterion. Sensors, 20(24), 7185. https://doi.org/10.3390/s20247185

Lin, Y.-B., Lee, F.-Z., Chang, K.-C., Lai, J.-S., Lo, S.-W., Wu, J.-H., & Lin, T.-K. (2021). The Artificial Intelligence of Things Sensing System of Real-Time Bridge Scour Monitoring for Early Warning during Floods. Sensors, 21(14), 4942. https://doi.org/10.3390/s21144942

Malekloo, A., Ozer, E., AlHamaydeh, M., & Girolami, M. (2022). Machine learning and structural health monitoring overview with emerging technology and high-dimensional data source highlights. Structural Health Monitoring, 21(4), 1906–1955. https://doi.org/10.1177/14759217211036880

Mishra, V., & Sadhu, A. (2023). Towards the effect of climate change in structural loads of urban infrastructure: A review. Sustainable Cities and Society, 89, 104352. https://doi.org/10.1016/j.scs.2022.104352

Ozsarac, V., Pereira, N., Mohamed, H., Romão, X., & O'Reilly, G. J. (2025). The Built Environment Data Framework for Simulated Design and Vulnerability Modelling in Earthquake Engineering. Earthquake Engineering & Structural Dynamics, 54(11), 2651–2670. https://doi.org/10.1002/eqe.4378

Pal, J., Sikdar, S., Banerjee, S., & Banerji, P. (2022). A combined machine learning and model updating method for autonomous monitoring of bolted connections in steel frame structures using vibration data. Applied Sciences, 12(21), 11107.

Prendergast, L. J., & Gavin, K. (2014). A review of bridge scour monitoring techniques. Journal of Rock Mechanics and Geotechnical Engineering, 6(2), 138–149. https://doi.org/10.1016/j.jrmge.2014.01.007

Rözer, V., Mehryar, S., & Surminski, S. (2022). From managing risk to increasing resilience: a review on the development of urban flood resilience, its assessment and the implications for decision making. Environmental Research Letters, 17(12), 123006. https://doi.org/10.1088/1748-9326/aca8bc

Sun, X., Ilanko, S., Mochida, Y., & Tighe, R. C. (2023). A Review on Vibration-Based Damage Detection Methods for Civil Structures. Vibration, 6(4), 843–875. https://doi.org/10.3390/vibration6040051

Zarafshan, A., Iranmanesh, A., & Ansari, F. (2012). Vibration-Based Method and Sensor for Monitoring of Bridge Scour. Journal of Bridge Engineering, 17(6), 829–838. https://doi.org/10.1061/(ASCE)BE.1943-5592.0000362